Electric Power Systems Research 190 (2021) 106779

Contents lists available at ScienceDirect

Electric Power Systems Research

journal homepage: www.elsevier.com/locate/epsr

Analysis of synchronization in load ensembles

Md Salman Nazir*, Ian Hiskens

Department of Electrical Engineering and Computer Science, University of Michigan, Ann Arbor, MI, USA

ARTICLE INFO

Keywords:
Demand response
Modal analysis
Load control
Synchronization
Thermostatically controlled loads

ABSTRACT

While coordinated control of a large population of electric loads can provide important services to the electric grid, situations have been observed where control of load ensembles may lead to highly nonlinear behavior such as synchronization, sustained oscillations and bifurcations. Synchronization of thermostatically controlled loads (TCLs) is undesirable since it can lead to increased short-cycling, sudden changes in power demand and network voltage issues. In this paper, we investigate the synchronizing tendency of TCLs under control strategies where updates are broadcast periodically for coordinating TCLs. We study the problem using a hybrid dynamical systems framework to model both the continuous and discrete dynamics of load ensembles. Analysis of eigenmodes of the underlying discrete-time system provide insights into synchronizing tendencies and rate of convergence to the synchronized state. Simulations are provided to illustrate the theory.

1. Introduction

Coordinated control of thermostatically controlled loads (TCLs), such as air-conditioners, water-heaters and refrigerators, can provide many services to power systems, including balancing fluctuations from renewables, reducing peak demand and providing voltage support [1,2]. Various coordination techniques have been proposed in the literature including randomized switching, temperature set-point variation, and Transactive energy coordination. However, such controls may sometimes lead to undesirable phenomenon such as synchronization (which generally refers to the loss of diversity in temperatures) of TCLs and large fluctuations in aggregate demand of loads [3–6]. Large oscillations in aggregate power may cause new peaks in system demand and result in voltage violations in distribution systems. TCL synchronization can additionally lead to increased short-cycling of TCLs, sudden undesirable changes in power demand, and poor performance of TCL controllers [7–9]. Hence, synchronizing behavior of TCLs under different control schemes must be carefully studied.

1.1. Literature review

Temperature synchronization of TCLs is a well-known problem, especially in the context of demand response (DR) events where applying a prolonged 'off' signal to TCLs causes loss of natural diversity. Consequently at the end of the DR event, new peaks and oscillations are observed [4,10]. However, synchronization of TCL temperatures is less studied and understood under advanced coordination mechanisms, such as market-based coordination, set-point variation and randomized switching, where control signals may be updated regularly with update intervals varying from a few seconds to minutes ranges. A systematic analysis of such cases is therefore the main focus of our work.

Since the ensemble behavior of hysteresis-based loads is challenging to model, simulation-based studies are often undertaken to show the possibility of oscillations and characterize the damping due to noise and heterogeneity. In [1], oscillatory behavior was observed in the aggregate demand when simulating a large number of price-responsive electric vehicles. In [5,8], simulations show that under market-based coordination of TCLs, a sequence of price signals can induce synchronization and large oscillations in the aggregate TCL demand. Synchronization and rapid cycling of TCLs may also appear under randomized switching schemes, hence has been studied in [7]. Some recent work [11–13] provides analytical results characterizing the behavior of TCLs in the presence of noise and heterogeneity. However, the synchronizing and oscillatory behavior observed in [8,14], [14] cannot be explained fully without resorting to modeling both the continuous-time behavior of loads as well as the discrete events due to the control actions that occur at slower intervals. Hence, the reset-based hybrid systems model presented in this paper can provide intuition into complex system behavior which is not available under simplifying modeling assumptions that are common in the existing literature.

1.2. Contributions

The paper presents an analytical investigation of conditions under

* Corresponding author.
E-mail addresses: mdsnazir@umich.edu (M.S. Nazir), hiskens@umich.edu (I. Hiskens).

https://doi.org/10.1016/j.epsr.2020.106779
Received 5 October 2019; Received in revised form 20 April 2020; Accepted 2 August 2020
Available online 18 September 2020
0378-7796/

which temperature synchronization of TCLs may appear and large oscillations in the aggregate demand of a load ensemble may emerge. For understanding oscillatory behavior with TCLs, under a given control strategy, it is important to understand if the control has a tendency to synchronize the TCLs, and to what degree. We show that eigenmode analysis can (i) guarantee if synchronization will appear, (ii) the rate at which it would appear. To accomplish this, the dynamics of a controlled TCL population, under a given strategy, is expressed using a reset-based hybrid system. This allows us to study the problem as a parameter-dependent eigenvalue problem. Using the hybrid representation, the aggregate autonomous dynamics of TCLs is captured using a continuous-time model while the control updates (e.g. price or set-point updates) are assumed to occur at slower discrete intervals (minutes range). Then, the eigenvalues and steady-state distributions of a discretized system are analyzed to explain the effects of control input variations, check if synchronization is imminent, and find bounds on demand fluctuations. A set of indices to automatically measure synchronization has also been proposed. Then, for both priority- or market-based control and randomized switching, we show how control update intervals and levels of control variations can influence periodic behavior, synchronization, and/or damping of oscillations. For a given initial condition, modal analysis can also lead to reduced computational needs.

The remainder of the paper is organized as follows. Section 2 describes the modeling and control framework. Section 3 presents modal analysis to characterize the systems. Section 4 proposed a set of indices to automatically measure synchronization. Section 5 provides numerical examples. Finally, Section 6 concludes by summarizing our findings and discussing their implications.

2. Modeling TCL dynamics as a reset-based hybrid system

2.1. Individual TCL model

The temperature, $\theta(t)$ (in ˚C) dynamics of TCLs can be modeled using a first-order differential equation [3,10,15],

$$\dot{\theta}(t) = \frac{1}{CR}\left(\theta^{\text{amb}} - \theta(t) - m(t)PR\right) \tag{1}$$

where C is the thermal capacitance (kWh/˚C), R is the thermal resistance (˚C/kW), P is the energy transfer rate which is positive for cooling TCLs (e.g. air-conditioners), θ^{amb} (˚C) is the ambient temperature external to the conditioned space. The on/off state $m(t)$ is governed by the thermostatic switching law with a dead-band, δ^{db} (˚C), around a user-specified set-point, θ^{set} (˚C). Then, $\theta^{\min} = \theta^{\text{set}} - \delta^{\text{db}}/2$, $\theta^{\max} = \theta^{\text{set}} + \delta^{\text{db}}/2$, and

$$m(t) = \begin{cases} 0, & \text{if } \theta(t) \le \theta^{\min} \\ 1, & \text{if } \theta(t) \ge \theta^{\max} \\ m(t^-), & \text{otherwise,} \end{cases} \tag{2}$$

where t^- represents the limit from below, since $m(t)$ is discontinuous at the switching times [16].

2.2. TCL population model

Following the work of [17–20], the autonomous dynamics of a TCL population can be described using an LTI system representation. The temperature range $[\theta^{\min}, \theta^{\min}]$ is first discretized using N bins, where the bin width is given by $\Delta^{\text{bw}} = \frac{\delta^{\text{db}}}{N}$. To capture both ON and OFF states, let bins $i = 1, \ldots, N$ represent the OFF states and $i = N+1, \ldots, 2N$ the ON states, as shown in Fig. 1. Let $x_i(t)$ represent the fraction of the total population of TCLs lying in bin i at time t. This implies $x_i(t) \ge 0$ and $\sum_{i=1}^{2N} x_i(t) = 1$ for all time $t \ge 0$. For convenience, we will use $\sum_{i=1}^{2N} x_i(t) = \mathbb{1}_{2N}^{\text{T}} x(t)$ where $\mathbb{1}_{2N}$ is the $2N$-length vector of all ones.

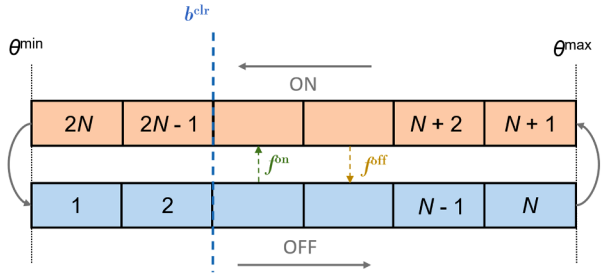

Fig. 1. Bin-based aggregate model for a TCL population. The influence of market-based strategies can be captured using b_{clr}, and the influence of randomized switchings can be captured using f^{on} or f^{off}.

The evolution of $x(t)$ can be described by,

$$\dot{x}(t) = \mathcal{A}x(t), \tag{3}$$

where the elements of matrix $\mathcal{A}$ can be obtained by considering the portion of the population of TCLs that is entering and leaving each bin [17–19]. Consider α_0 and α_1 to be the average OFF and ON rates of cooling TCLs, respectively. From (1), these rates can be approximated by [17,19], ,

$$\alpha_0 = \frac{1}{CR}\left(\theta^{\text{amb}} - \theta^{\text{set}}\right), \tag{4}$$

$$\alpha_1 = \frac{1}{CR}\left(\theta^{\text{amb}} - \theta^{\text{set}} - PR\right). \tag{5}$$

Then, for bins $2 \le i \le N$ and $N+2 \le i \le 2N$ we obtain,

$$\dot{x}_i(t) = \frac{\alpha_0}{\Delta^{\text{bw}}}\left(x_{i-1}(t) - x_i(t)\right), \quad 2 \le i \le N, \tag{6a}$$

$$\dot{x}_i(t) = \frac{\alpha_1}{\Delta^{\text{bw}}}\left(-x_{i-1}(t) + x_i(t)\right), \quad N+2 \le i \le 2N, \tag{6b}$$

and for the bins, $i = 1$ and $i = N+1$, at the $\theta^{\min}$ and $\theta^{\max}$ boundaries, respectively, we obtain,

$$\dot{x}_1(t) = -\frac{\alpha_0}{\Delta^{\text{bw}}}x_1(t) - \frac{\alpha_1}{\Delta^{\text{bw}}}x_{2N}(t); \tag{7a}$$

$$\dot{x}_{N+1}(t) = -\frac{\alpha_0}{\Delta^{\text{bw}}}x_N(t) + \frac{\alpha_1}{\Delta^{\text{bw}}}x_{N+1}(t). \tag{7b}$$

The coefficients in (6) and (7) give the elements of $\mathcal{A}$.

Because (3) is a linear time-invariant (LTI) system, its solution can be written explicitly as,

$$x(t+\tau) = \exp(\mathcal{A}\tau)x(t).$$

For subsequent development of a discrete-time equivalent of (3), it is convenient to define,

$$A = \exp(\mathcal{A}). \tag{8}$$

By construction, the matrix A is the transpose of a Markov transition matrix [21].

The discrete-time A-matrix can also be obtained from Monte Carlo simulation of (1) and (2) [21]. Techniques to incorporate noise and heterogeneity are presented in [12,22].

2.3. Controlled dynamics as a reset-based hybrid system

In earlier work on TCL control design, state space models have assumed control action is applied at every time-step. However, the control updates typically occur at relatively slow discrete intervals, whereas the aggregate dynamics of TCLs are more accurately captured using continuous-time models. This time-scale separation of the continuous/discrete dynamics of TCLs coordinated by switching signals can

be expressed as:

$$\dot{x}(t) = \mathcal{A}x(t), \quad \text{(continuous dynamics)} \tag{9a}$$

$$x(t) = B(t)x(t^{-}),\ t = \tau,\ 2\tau,\ \cdots \quad \text{(discrete switching)} \tag{9b}$$

$$y(t) = Cx(t). \quad \text{(output)} \tag{9c}$$

In (9b), it is assumed that discrete switching occurs only at $t = \tau, 2\tau, ...,$ where τ is the switching interval. The effect of control action is captured by the reset matrix $B(t)$, with the entries of $B(t)$ dependent on the particular control strategy. Sections 2.4 and 2.5 develop B-matrices for randomized switching, and for market- and priority-based strategies.

With $\mathcal{A}$ time-invariant and A its discrete-time equivalent, the evolution of $x(t)$ from one reset event to the next is given by,

$$x(t+\tau) = B(t)A^{\tau}x(t), \quad t = 0, \tau, 2\tau, ... \tag{10}$$

This can be expressed in discrete-time as,

$$x^{+}((k+1)\tau) = x_{k+1} = B_k A^{\tau} x_k, \quad k = 0, 1, 2, ..., \tag{11}$$

where k indexes the discrete intervals and x^{+} represents the TCL distribution immediately after a reset.

The hybrid model (9a)–(9c) is sufficiently general to support a variety of control strategies, such as randomized switching, market-based coordination and set-point variation. The reset map and switching interval depends on the particular strategy.

2.4. Randomized switching

Sending probabilistic switching signals to increase/decrease power consumption has frequently been considered in TCL literature [9,16,20,21]. Consider control logic where bins receive a command signal to switch the status of a fixed fraction of the bin's TCLs (during dispatch each TCL can generate a random number and turn on/off to meet this signal [9,21]). For a power increase, where the fraction f^{on} of the bin's TCLs are switched from off to on, the reset equations can be written,

$$x_i^{+} = (1 - f^{\text{on}})x_i^{-}, \quad 1 \le i \le N, \tag{12a}$$

$$x_i^{+} = x_i^{-} + f^{\text{on}}x_{2N-i+1}^{-}, \quad (N+1) \le i \le 2N, \tag{12b}$$

where the superscripts - and + refer to the value taken by the state just prior to and just after the reset event, respectively. For a power decrease, where the fraction f^{off} of TCLs within a bin are switched from on to off, the reset equations are,

$$x_i^{+} = x_i^{-} + f^{\text{off}}x_{2N-i+1}^{-}, \quad 1 \le i \le N, \tag{13a}$$

$$x_i^{+} = (1 - f^{\text{off}})x_i^{-}, \quad (N+1) \le i \le 2N. \tag{13b}$$

The reset matrices B^{on} associated f^{on} and B^{off} associated f^{off} can be readily obtained from the above. The column sums for B^{on} and B^{off} equal 1 to ensure probability conservation.

2.5. Market- or priority-based scheme

As detailed in [6], market-based or transactive techniques for coordinating TCLs can be incorporated in the aggregate model using reset equations. Assume TCLs that reach higher temperatures are willing to pay increasingly higher prices to turn on than those already at cooler temperatures [6,23]. Upon broadcast of a price signal, TCLs with offers above the market price will clear. In the bin model, this means (i) TCL price offers increase from lower temperature bins to higher bins, and (ii) on/off bins at the same temperature have the same offer price, hence are cleared simultaneously. A clearing price $\pi^{\text{clr}}(t)$ thus determines which bins are *cleared* (i.e. allowed to turn ON to consume power). Note that the above coordination mechanism is conceptually similar to the 'priority-stacking' scheme [2,21] where bins near the edges get progressively higher priority to switch on/off depending on whether they are near the upper/lower limit of the dead-band range.

Assume each bin i has a corresponding price level π_i. Assume a market-clearing price π^{clr}, with $b^{\text{clr}} \in \{1,...,N\}$ being the clearing bin index associated with π^{clr}. Then, for $i \in \{b^{\text{clr}}+1, ...,N\}$, the price $\pi_i \ge \pi^{\text{clr}}$, so all such bins get cleared (see Fig. 1). On the other hand, bins $i \in \{1, ...,b^{\text{clr}}\}$ do not get cleared. The ON bins corresponding to each OFF bin behave similarly because $\pi_i = \pi_{2N-i+1}$ for $i = 1, ...,N$. Hence, the reset equations can be written,

$$x_i^{+} = x_i^{-} + x_{2N-i+1}^{-}, \quad 1 \le i \le b^{\text{clr}}, \tag{14a}$$

$$x_i^{+} = 0, \quad (b^{\text{clr}}+1) \le i \le N, \tag{14b}$$

$$x_i^{+} = x_i^{-} + x_{2N-i+1}^{-}, \quad N+1 \le i \le (2N - b^{\text{clr}}), \tag{14c}$$

$$x_i^{+} = 0, \quad (2N - b^{\text{clr}} + 1) \le i \le 2N. \tag{14d}$$

Eq. (14) form the B-matrix for this control scheme. The column sum of B is always equal to 1 to ensure probability conservation. In a market-based coordination framework, the clearing prices $\pi^{\text{clr}}(t)$ can vary with time t. Different clearing prices $\pi^{\text{clr}}(t)$ result in different clearing bins $b_{\text{clr}}(t)$ The corresponding $B(t)$ follows from (14).

In the following section, we develop an eigenvalue-based approach to analyze how system behavior changes as TCL parameters change and under different control strategies.

3. Analysis using eigenmodes

3.1. Modal decomposition

Modal analysis of $\mathbb{A} = BA^{\tau}$ can be used to explore the evolution of TCLs under periodic control. Assume matrix $\mathbb{A}$ is diagonalizable, with eigenvalues $\lambda_1, \lambda_2, ...,\lambda_{2N}$ and corresponding right eigenvectors $v_1, v_2, ...,v_{2N}$, i.e. $\mathbb{A}v_i = \lambda_i v_i$. Let $V = [v_1\ v_2\ ...\ v_{2N}]$.

Matrix A is the transpose of a Markov transition matrix and B is structured to ensure $\mathbb{1}_{2N}^{T}x = 1$. Therefore, $\mathbb{A}$ is also the transpose of a transition matrix. Accordingly, it has one eigenvalue at 1 (its largest) [24]. The eigenvalues can be ordered $1 = \lambda_1 \ge |\lambda_2| \ge ....\ge |\lambda_{2N}|$.

Let $c = V^{-1}x_0$. Then it is straightforward to show that the initial condition x_0 can be expressed as,

$$x_0 = c_1 v_1 + ... + c_{2N} v_{2N}. \tag{15}$$

Therefore,

$$x_k = \mathbb{A}^k x_0 = \sum_{i=1}^{2N} c_i \lambda_i^{\,k} v_i. \tag{16}$$

Hence, x_k can be decomposed into the weighted sum of the temporal evolution of each eigenmode. The eigenmodes may involve complex c_i, λ_i, v_i depending on the structure of $\mathbb{A}$. Such complex valued eigenmodes contribute to x_k in conjunction with their complex conjugate, which must also be an eigenmode because $\mathbb{A}$ is a real-valued matrix. The contribution to x_k from this pair of complex conjugate modes can be expressed as,

$$x_k = 2|c_i||\lambda_i|^k|v_i|\cos(k \times \angle\lambda_i + \angle c_i + \angle v_i), \tag{17}$$

where $|v_i|$ and $\angle v_i$ refer to the vector that satisfy $v_i = |v_i|\angle v_i$ on an element-by-element basis.

Because $\lambda_1 = 1$, the first mode $c_1 v_1$ describes the steady-state distribution of TCLs across the bins, with $c_1 \mathbb{1}_{2N}^{T} v_1 = 1$. Furthermore, due to the structure of $\mathbb{A}$, all other modes $i = 2, ...,2N$ satisfy $\mathbb{1}_{2N}^{T} v_i = 0$. For modes with $|\lambda_i| < 1$, it can be seen from (16) and (17) that the modal contribution will decay to zero. It is possible for $\lambda_2 = -1$, or more generally $|\lambda_i| = 1$ for $i \ge 2$ (though this is rare beyond $i = 2$). Such modes will not decay, but rather introduce an undamped oscillation that adds to the steady-state mode $c_1 v_1$. It is also interesting to note that if $x_0 - c_1 v_1$ lies on a real eigenvector v_i then the deviation from steady-

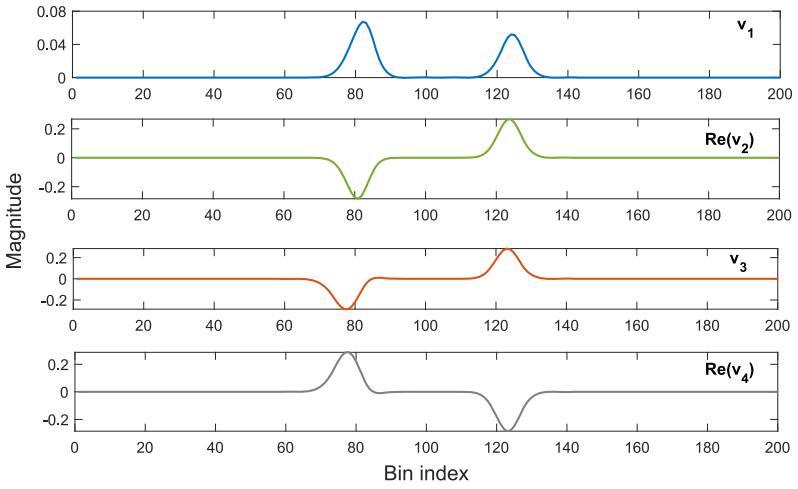

Fig. 2. Mode shapes for four modes.

state $c_1 v_1$ will always lie on v_i. For complex eigenvectors, if $x_0 - c_1 v_1$ lies on the plane spanned by the vectors $\mathrm{Re}(v_i)$ and $\mathrm{Im}(v_i)$ then the deviation from steady-state will always lie on that plane.

Mode shapes (eigenvectors) of the first four mode for a typical TCL-derived $\mathbb{A}$-matrix are shown in Fig. 2. As mentioned previously, the first mode describes the steady-state distribution while the other modes influence the transient behavior. For the two complex modes, 2 and 4, the real portion has been plotted.

3.2. Convergence rate analysis

Synchronization of TCLs is dependent upon particular coordination strategies. The steady-state distribution of TCLs is described by the eigenvector v_1, the first mode of $\mathbb{A}$, so it determines whether or not synchronization will occur. The convergence rate to a synchronized state is directly related to the eigenvalues of $\mathbb{A}$.

From (16) and (17), if $|\lambda_2| < 1$, $\mathbb{A}^k x_0 \to c_1 v_1$ since $\lambda_2^k \to 0$ as $k \to \infty$. Thus, x_k converges to a multiple of eigenvector v_1 such that the elements of $c_1 v_1$ sum to 1. The convergence is geometric with ratio $\frac{|\lambda_2|}{|\lambda_1|} = |\lambda_2|$. This is illustrated in Fig. 3 for a range of $|\lambda_2|$ values and evolution in k. In certain cases, $\lambda_2 = -1$ (as will be shown in Section 5). Then, x_k will oscillate as noted earlier.

After k time steps, let $|\lambda_2|^k = \epsilon$, where ϵ is small. Taking logs of both sides gives,

$$k(\epsilon) = \left[\frac{\log(\epsilon)}{\log(|\lambda_2|)}\right]. \tag{18}$$

For example, with $\epsilon = 10^{-5}$ and $\lambda_2 = 0.5$, we obtain $k = 17$. With $\lambda_2 = 0.2$ we obtain $k = 8$. Thus, the contribution of λ_2 vanishes in a limited number of time-steps.

More generally, since $\mathbb{A}$ can be shown to be the transpose of a Markov transition matrix, the convergence behavior can also be studied using the spectral gap γ^* of matrix $\mathbb{A}$, where $\gamma^* = 1 - |\lambda_2|$. Large gaps indicate faster convergence [24].

3.3. Bounds on variations in aggregate power

Eigenmode analysis can also be used to obtain bounds on aggregate power variations for controlled TCL ensembles.

3.3.1. Fixed reset conditions

Assume B is fixed and dynamics are governed by $\mathbb{A} = BA^\tau$. The steady-state when observed just after the reset, denoted x_{ss}^+, is given by v_1 of $\mathbb{A}$. The steady-state observed just prior to the reset x_{ss}^- is related through $x_{ss}^+ = Bx_{ss}^-$. Thus, at resets (when the control update is applied), the absolute change in power consumed by TCLs can be obtained using,

$$|y^+ - y^-| = |C(x_{ss}^+ - x_{ss}^-)| \tag{19a}$$

$$= |C(B - I)x_{ss}^-|. \tag{19b}$$

3.3.2. Variable reset conditions

Variable reset conditions can also be considered. For example, it is straightforward to extend to the case of periodic reset signals where two reset maps B_1 and B_2 are applied alternatively during reset events. In this case, the dynamics can be written in either of the two forms,

$$x_{k+1} = B_1 A^\tau B_2 A^\tau x_k, \quad k = 0, 1, 2, \ldots, \tag{20a}$$

$$x_{k+1} = B_2 A^\tau B_1 A^\tau x_k, \quad k = 0, 1, 2, \ldots. \tag{20b}$$

The steady-state distribution corresponding to x_{ss}^+ is given by the eigenvector v_1 of $B_1 A^\tau B_2 A^\tau$ or $B_2 A^\tau B_1 A^\tau$. Knowing x_{ss}^- and x_{ss}^+, the change in aggregate power consumed can be computed without resorting to

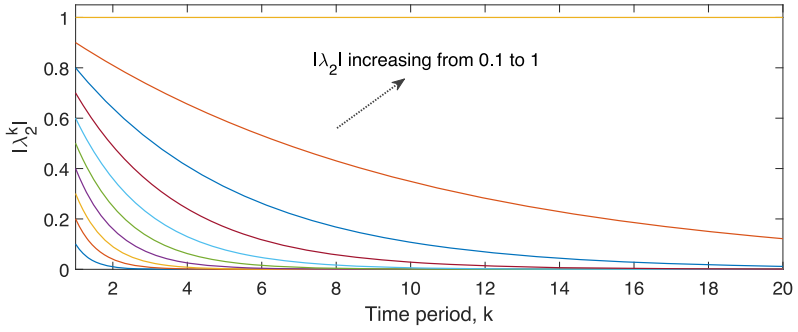

Fig. 3. Eigenvalue convergence, considering λ_2 from 0.1 to 1 and plotting λ_2^k, $k = 1, \ldots, 20$.

simulation. The above technique can also be extended to study other combinations of control sequences.

4. Synchronization index

While it is intuitive to detect full or partial synchronization of TCL temperature distributions by visual inspection, it can be time-consuming and does not provide a quantifiable result. Availability of standard and easy to interpret indices would allow systematic measurement of the level of synchronization in a given TCL distribution, and indicate if mitigating actions should to be taken. For example, it may be appropriate to implement feedback or penalty terms to suppress synchronization. In order to propose such measures, recall that a bin represents a temperature range and its associated on/off state. The temperature distribution x^θ over the bin space can be reconstructed using,

$$x_i^\theta = x_i + x_{2N-i+1}, \quad i = 1, \ldots, N, \tag{21}$$

because i and $2N - i + 1$, $i = 1, \ldots, N$ represent the same temperature range. Using x^θ, the following synchronization indices are proposed:

4.1. Maximum fraction of TCLs in a bin

Given a distribution x^θ over N bins, $S_1 \in [0\ 1]$ is given by,

$$S_1 = \max\{x_i^\theta,\ i = 1, \ldots, N\}. \tag{22}$$

4.2. Bin spread

Define $\mathcal{X}_\epsilon$ as a set of indices of bins containing TCL fractions above a specified threshold ϵ. Hence,

$$\mathcal{X}_\epsilon = \{i\colon x_i^\theta \geq \epsilon,\ i = 1, \ldots, N\}. \tag{23}$$

Then, a measure for bin spread is given by the cardinality of $\mathcal{X}_\epsilon$, i.e. $|\mathcal{X}_\epsilon|$. Normalizing gives,

$$S_2 = 1 - \frac{|\mathcal{X}_\epsilon|}{N}, \tag{24}$$

with $S_2 \in [0\ 1]$. Small values of S_2 indicates the distribution is widely spread over the temperature bins, whereas larger values indicate synchronization.

4.3. Bin range

Note however that S_2 as a measure of the bin spread is still not indicative of whether fractions of TCLs are lying in adjacent bins or are spread apart. Hence, the range the of $\mathcal{X}_\epsilon$ should also be considered,

$$S_3 = 1 - \frac{\max \mathcal{X}_\epsilon - \min \mathcal{X}_\epsilon}{N}, \tag{25}$$

giving $S_3 \in [0\ 1]$. Smaller values of S_3 imply TCL distributions are more widely spread over bins, whereas larger values indicate synchronization.

4.4. Combined metric

Each of the indices $0 \leq S_1, S_2, S_3 \leq 1$ can be measured and reported separately. However, since all are normalized quantities, consider the combined indices,

$$\hat{S} = S_1 S_2 S_3. \tag{26}$$

or alternatively,

$$S_t = \frac{\omega_1 S_1 + \omega_2 S_2 + \omega_3 S_3}{\omega_1 + \omega_2 + \omega_3}, \tag{27}$$

where the ω_i are user-defined weights. While more sophisticated measures can also be considered, this paper will consider the listed three.

These proposed indices, together with convergence rates from eigenvalues and spectral gaps, provide detailed insights into whether a given control strategy will induce synchronization, to what degree and at what rate.

5. Simulations

5.1. Influence of parameters on system behavior

Consider $N = 200$. To obtain the $\mathcal{A}$-matrix, the average heating and cooling rates in (4) and (5) are computed using $P = 14$ kW, $R = 2$ °C/kW, $C = 10$ kWh/°C, $\theta^{\text{set}} = 20$ °C and $\theta^{\text{amb}} = 32$ °C [3] (unless specified otherwise). A 2 °C dead-band is assumed. Then, the A matrix is obtained from $\mathcal{A}$ using (8). Matrix B for market-based switching is calculated using b^{clr} and for randomized switching (RS) using f^{on} and f^{off}.

To study how system behavior changes under market-based switching with changes in TCL parameters, three cases are considered,

(a) $\tau = 30$ min and $b^{\text{clr}} = 0.8N$,
(b) $\tau = 10$ min and $b^{\text{clr}} = 0.8N$,
(c) $\tau = 30$ min and $b^{\text{clr}} = 0.5N$.

For cases (a)–(c), we vary θ^{amb} from 21 to 40 °C. For each θ^{amb}, we compute α_0 and α_1, construct the A-matrix, and apply B to obtain $\mathbb{A}$ (see (11)). For case (a), the changes in real and imaginary parts of the eigenvalues are shown in Figs. 4 and 7, as a function of $|\alpha_0/\alpha_1|$ (which changes due to changing θ^{amb}). Similarly, for case (b), the changes in real and imaginary parts of the eigenvalues are shown in Figs. 5 and 9, and for case (c), in Figs. 6 and 9.

In case (a), we observe that as $|\alpha_0/\alpha_1|$ increases, an eigenvalue of value -1 emerges. For these parameter values, if this second mode is excited by the initial conditions x_0, it will introduce sustained oscillations about the steady-state distribution $c_1 v_1$ described by the first mode. Only when the initial conditions x_0 do not have a component in the direction of the eigenvector v_2 of the second mode, i.e. $c_2 = 0$ in (15), will the bins converge to the steady-state distribution. From Figs. 7–9, we also notice how the imaginary parts of the eigenvalues disappear when $|\alpha_0/\alpha_1|$ approaches 1, indicating structural changes in the system behavior.

Fig. 13 shows the values of the synchronization index $\hat{S}$ (given by (26)) for cases (a)–(c). Additionally, for case (a), Fig. 14 shows the individual indices (S_1, S_2, S_3). In case (a), with $\tau = 30$ min, we observe that $\hat{S}$ generally increased with increasing $|\alpha_0/\alpha_1|$. While S_1, which indicates the maximum TCL concentration in a single bin, did not vary considerably, the values of S_2 and S_3, indicating the bin spread and bin ranges, showed some increase as $|\alpha_0/\alpha_1|$ increased. From Figs. 13 and 14, it is confirmed that $\hat{S}$ effectively captures the behavior of the

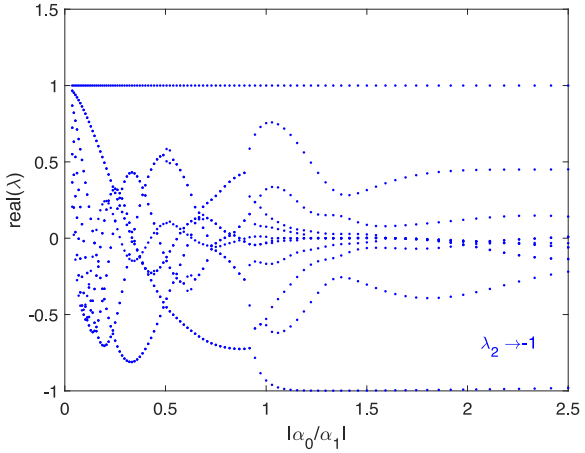

Fig. 4. Real parts of eigenvalues as a function of $|\alpha_0/\alpha_1|$ in case (a).

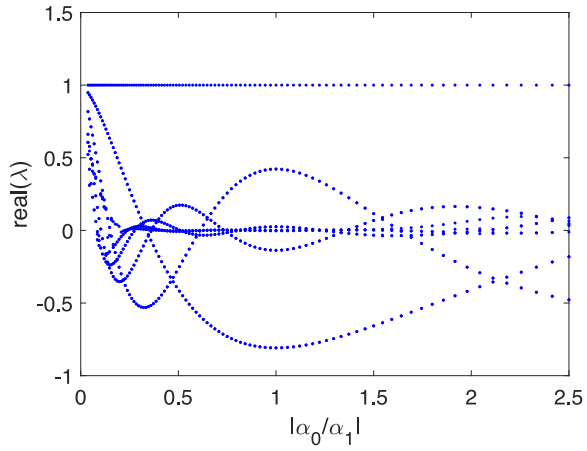

Fig. 5. Real parts of eigenvalues as a function of $|\alpha_0/\alpha_1|$ in case (b).

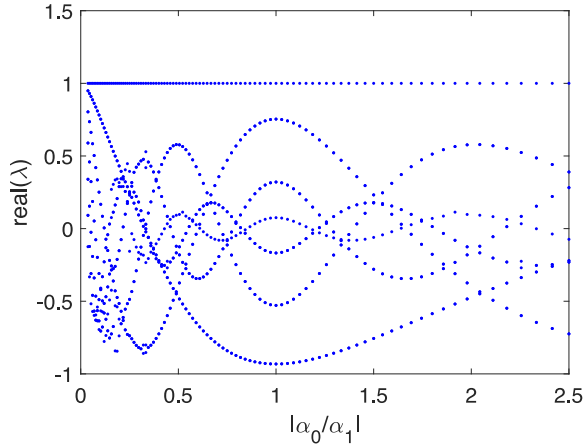

Fig. 6. Real parts of eigenvalues as a function of $|\alpha_0/\alpha_1|$ in case (c).

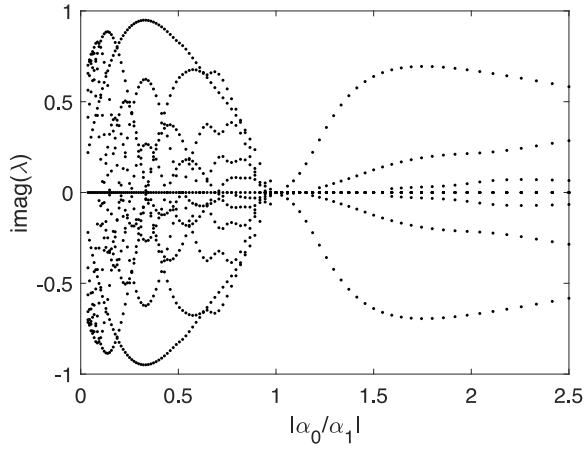

Fig. 7. Imaginary parts of eigenvalues as a function of $|\alpha_0/\alpha_1|$ in case (a).

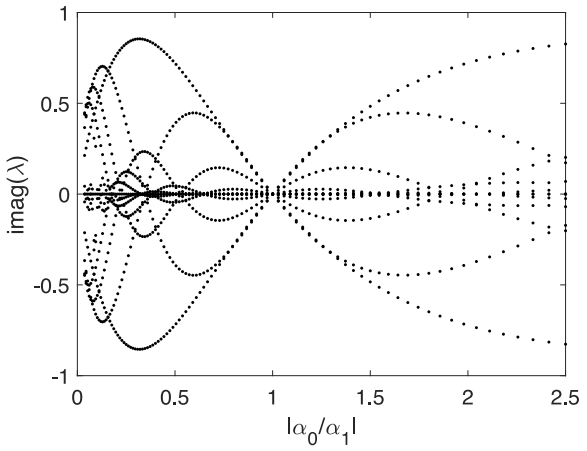

Fig. 8. Imaginary parts of eigenvalues as a function of $|\alpha_0/\alpha_1|$ in case (b).

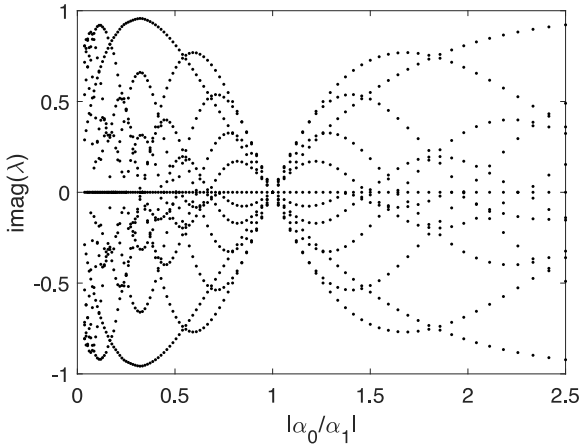

Fig. 9. Imaginary parts of eigenvalues as a function of $|\alpha_0/\alpha_1|$ in case (c).

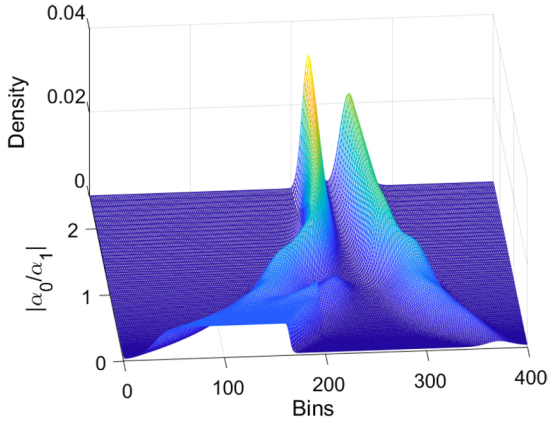

Fig. 10. Steady-state distribution as a function of $|\alpha_0/\alpha_1|$ in case (a).

individual indices without being overly sensitive to changes in any single index. These indices thus enable us to rapidly quantify synchronizing behavior in TCL ensembles without resorting to visual inspections of the steady-state distributions (Figs. 10–12).

In cases (b) and (c), $|\lambda_i| < 1$ for $\forall i > 1$. Hence, unlike in case (a), x_k will always converge to the steady-state given by $c_1\lambda_1$. From Fig. 13, observe that $\hat{S}$ remains relatively constant. This is because with $\tau = 10$ min, the TCL distributions remain synchronized around b^{clr} (also see Fig. 11). In case (c), however, with $\tau = 30$ min and $b^{\text{clr}} = 0.5N$, TCLs can propagate further away from b^{clr}, hence the value of $\hat{S}$ remained low (see Fig. 12). While in case (a), τ was also 30 min, b^{clr} was close to the temperature boundary, hence temperatures did not propagate further away from b^{clr} since TCLs reaching the boundary within τ switched their on/off states. Finally, it was observed that for case (b), the peak value of the spectral radius $(1 - |\lambda_2|)$ was at 0.35 (when $|\alpha_0/\alpha_1| = 1$), much higher than 0.13 observed for cases (a) and (c), suggesting faster convergence to the synchronized state for case (b).

Comparing cases (a)–(c), it can be summarized that when b^{clr} lay near the temperature boundaries and when τ was relatively small, the tendency to synchronize remained relatively higher. These simulations thus show how the synchronizing behavior of TCL ensembles under

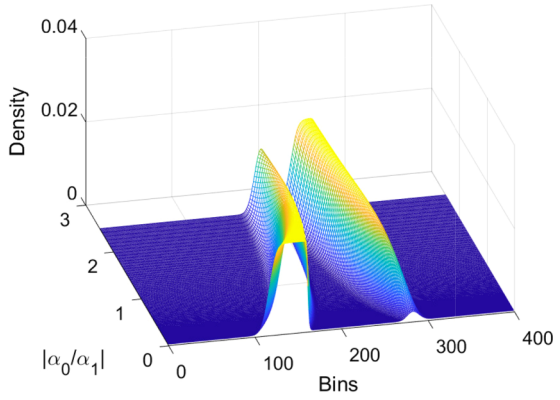

Fig. 11. Steady-state distribution as a function of $|\alpha_0/\alpha_1|$ in case (b).

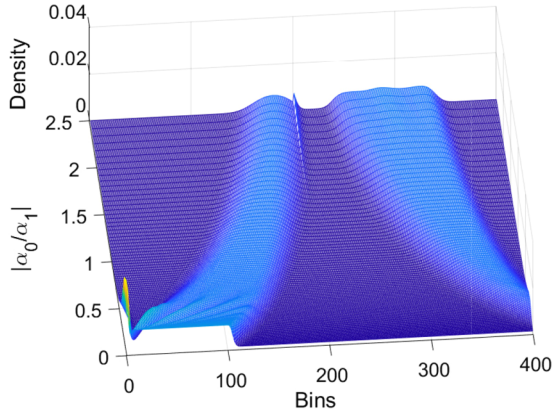

Fig. 12. Steady-state distribution as a function of $|\alpha_0/\alpha_1|$ in case (c).

market-clearing can be efficiently captured by analyzing the impact of varying b^{clr}, τ and $|\alpha_0/\alpha_1|$ using the proposed eigenmode based techniques.

Next, we performed a similar analysis for randomized switching (RS) based coordination. A fraction of TCLs in each bin are asked to periodically increase and subsequently decrease power consumption, where each increase or decrease phase lasts for T minutes. Three cases are considered,

(i) $f^{\text{on}} = 0.001$, $f^{\text{off}} = 0.001$, $T = 5$ min,
(ii) $f^{\text{on}} = 0.001$, $f^{\text{off}} = 0.001$, $T = 10$ min,
(iii) $f^{\text{on}} = 0.0001$, $f^{\text{off}} = 0.0001$, $T = 5$ min.

First, B^{on} is constructed using f^{on} and B^{off} using f^{off}. Then, the evolution of x_k is captured by $\mathbb{A} = (B^{\text{on}}A^{\tau})^{60T}(B^{\text{off}}A^{\tau})^{60T}$ and $\mathbb{A} = (B^{\text{off}}A^{\tau})^{60T}(B^{\text{on}}A^{\tau})^{60T}$, where τ is set to 1 s. The resulting synchronization indices are shown in Fig. 15. The indices were much higher for small values of $|\alpha_0/\alpha_1|$. This suggests, when θ^{amb} is low, α_0 is much smaller than α_1 (cooling rate is much faster since heating is slow due to low ambient temperature). Thus, under a symmetric and fixed up-down power request signal, the TCL temperatures may become highly synchronized, under which TCLs would undergo fast cycling. In case (ii), with longer time duration of $T = 10$ min, this was even more severe. The synchronization level was slightly lower in case (iii) due to f^{on} and f^{off} being smaller. Finally, given the same $|\alpha_0/\alpha_1|$ values, the value of the spectral radius was highest (around 0.33) in case (ii), suggesting faster convergence to the synchronized state than in cases (i) or (iii). While we showed the effectiveness of the eigenmode analysis technique for a simplistic case of RS-strategy, the approach can be extended to study and identify critical cases pertaining to more advanced controllers [7,21].

5.2. Dominant modes and convergence

In (16), with eigenvalues ordered according to their magnitude, the first few modes are often referred to as the dominant modes. We chose x_0 to be uniformly distributed over $2N = 100$ bins. Then, we simulated to obtain x_k at $k = 0, 1, ..., 5$. In Fig. 16, we compared the actual x_k against different number of modes summed to give approximations at $k = 5$. In this case, just the first and second modes were sufficient to obtain almost the exact distribution, whereas using just the first mode resulted in some error. The evolution in the ith mode's weights, i.e. $w_i = c_i\lambda_i^k$ is shown in Fig. 17 for the first 6 modes, with $\lambda_1 = 1$ and $\lambda_2 = -0.87$. We see that the evolution in the 2nd mode's weight is oscillatory and does not die out rapidly, hence is important to consider. Additionally, since many of the eigenvalues have negligible values, their contributions are also negligible. Therefore, modal analysis and modal coordinates may provide significant computational advantages compared to simulating TCL dynamics using $2N \times 2N$ matrices. This is a topic of future research.

5.3. Bounds on aggregate power consumed

For a variety of control signals, the variations in output power can also be found using the eigenmodes. Assume TCLs are coordinated based on price signals in a double-auction market [6]. We applied periodic step changes in price signals, by varying b^{clr}, and observed different forms of oscillations in aggregate demand. Fig. 18 shows how a periodic price signal with small step changes induced large amplitude oscillations in the aggregate demand. The variations at resets matched the predicted value of 0.83 obtained via the method described in Section 3.3. Similarly, more complex signals can be constructed and variations in aggregate TCL power (at resets) can be obtained.

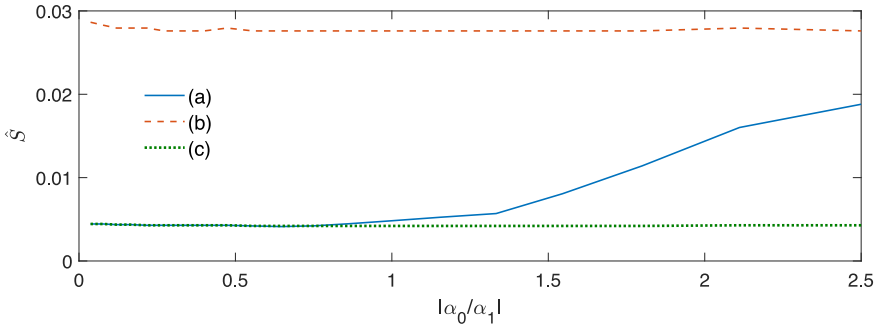

Fig. 13. Comparing the synchronization index values for cases (a)–(c) under market-based coordination.

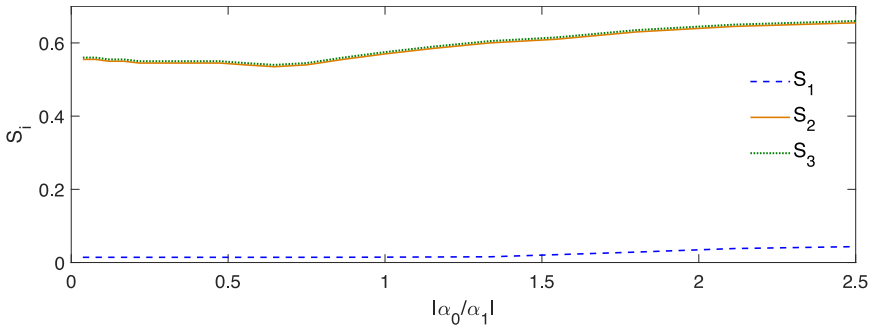

Fig. 14. Individual synchronization index values (S_1, S_2, S_3) for case (a) under market-based coordination.

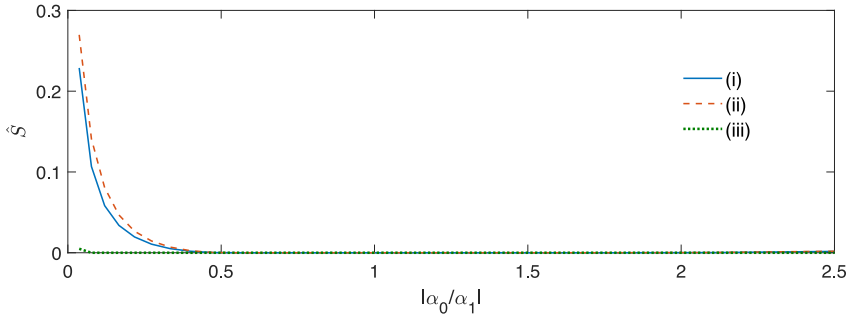

Fig. 15. Comparing the synchronization index values for cases (i)–(iii) under randomized switching signals.

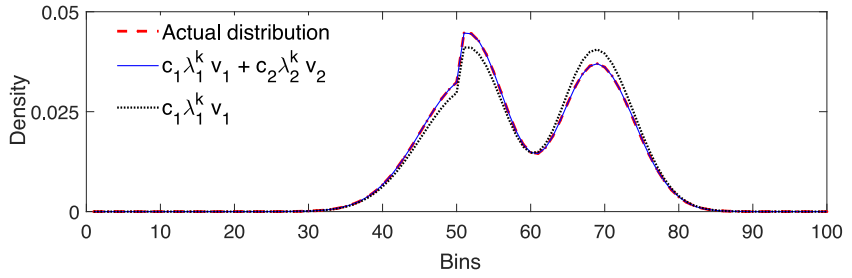

Fig. 16. At time period $k = 5$, actual TCL distribution (dashed line) vs. approximate distributions obtained using only 2 modes (solid line), only 1 mode (dotted line).

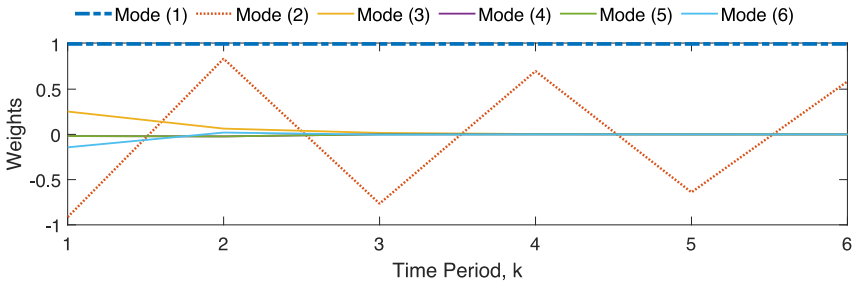

Fig. 17. Evolution in modal weights at discrete time intervals.

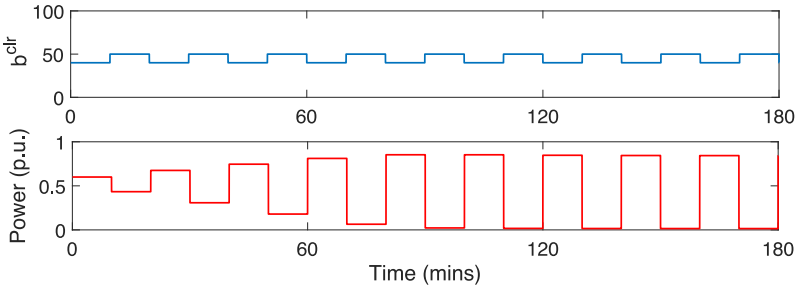

Fig. 18. Large fluctuations in demand induced by a periodic price signal (mapped to b^{clr}).

6. Conclusions

This paper presents an analytical framework to explore conditions under which temperature synchronization of TCLs may appear and large oscillations in aggregate demand of load ensembles may emerge. We show that eigen-structure analysis can (i) identify whether synchronization will appear, and (ii) determine the rate at which it would appear. To accomplish this, the dynamics of a controlled TCL population, under a given strategy, is expressed using a reset-based hybrid system. This allows us to study behavior as a parameter-dependent eigenvalue problem. The eigenvalues and steady-state distributions of the discretized system explain whether the control will induce synchronization. Under priority- or market-based control and randomized switching, we have shown that control parameters and update intervals can influence periodic behavior, synchronization, and/or damping of oscillations. The spectral gap of the transition matrix was used to estimate the convergence rate. The insights developed here can be used to quickly assess benefits and limitations of control techniques. Future work can involve comparing other control techniques and considering additional operational constraints such as lockouts.

Declaration of Competing Interest

The authors declare that they have no known competing financial interests or personal relationships that could have appeared to influence the work reported in this paper.

Acknowledgment

The authors gratefully acknowledge the contribution of the U.S. National Science Foundation through grant ECCS-1810144.

References

[1] D.S. Callaway, I.A. Hiskens, Achieving controllability of electric loads, Proc. IEEE 99 (1) (2011) 184–199.
[2] H. Hao, B.M. Sanandaji, K. Poolla, T.L. Vincent, A generalized battery model of a collection of thermostatically controlled loads for providing ancillary service, 51st Annual Allerton Conference on Communication, Control, and Computing, (2013), pp. 551–558.
[3] D.S. Callaway, Tapping the energy storage potential in electric loads to deliver load following and regulation, with application to wind energy, Energy Convers. Manag. 50 (5) (2009) 1389–1400.
[4] N.A. Sinitsyn, S. Kundu, S. Backhaus, Safe protocols for generating power pulses with heterogeneous populations of thermostatically controlled loads, Energy Convers. Manag. 67 (2013) 297–308.
[5] A.G. Thomas, L. Tesfatsion, Braided cobwebs: cautionary tales for dynamic pricing in retail electric power markets, IEEE Trans. Power Syst. 33 (6) (2018) 6870–6882.
[6] M.S. Nazir, I.A. Hiskens, A dynamical systems approach to modeling and analysis of transactive energy coordination, IEEE Trans. Power Syst. 34 (5) (2019) 4060–4070.
[7] A.R. Coffman, A. Busic, P. Barooah, Virtual energy storage from TCLs using QOS preserving local randomized control, Proceedings of the 5th Conference on Systems for Built Environments, (2018), pp. 93–102.
[8] M.S. Nazir, I.A. Hiskens, Load synchronization and sustained oscillations induced by transactive control, Proc. of the IEEE Power and Energy Society General Meeting, (2017).
[9] S. Nazir, S.C. Ross, J.L. Mathieu, I.A. Hiskens, Performance limits of thermostatically controlled loads under probabilistic switching, Proceedings of the 20th IFAC World Congress, Toulouse, (2017).
[10] R. Malhame, C.-Y. Chong, Electric load model synthesis by diffusion approximation of a high-order hybrid-state stochastic system, IEEE Trans. Autom. Control 30 (9) (1985) 854–860.
[11] D. Métivier, I. Luchnikov, M. Chertkov, Power of ensemble diversity and randomization for energy aggregation, Sci. Rep. 9 (1) (2019) 1–11.
[12] A. Ghaffari, S. Moura, M. Krstić, Modeling, control, and stability analysis of heterogeneous thermostatically controlled load populations using partial differential equations, J. Dyn. Syst. Meas. Control 137 (10) (2015) 1–9.
[13] D. Docimo, H. Fathy, Demand response using heterogeneous thermostatically controlled loads: characterization of aggregate power dynamics, J. Dyn. Syst. Meas. Control 139 (10) (2017) 1–9.
[14] S. Kundu, I.A. Hiskens, Nonlinear dynamics of hysteresis-based load controls, Proceedings of the 19th IFAC World Congress, Capetown, South Africa 47 (3) (2014) 5419–5425.
[15] S. Ihara, F.C. Schweppe, Physically based modeling of cold load pickup, IEEE Trans. Power Appar. Syst. PAS-100 (9) (1981) 4142–4150.
[16] L.C. Totu, R. Wisniewski, J. Leth, Demand response of a TCL population using switching-rate actuation, IEEE Trans. Control Syst. Technol. 25 (5) (2017) 1537–1551.
[17] S. Bashash, H.K. Fathy, Modeling and control insights into demand-side energy management through setpoint control of thermostatic loads, 2011 American Control Conference, (2011).
[18] S. Bashash, H.K. Fathy, Modeling and control of aggregate air conditioning loads for robust renewable power management, IEEE Trans. Control Syst. Technol. 21 (4) (2013) 1318–1327.
[19] S. Kundu, N. Sinitsyn, S. Backhaus, I. Hiskens, Modeling and control of thermostatically controlled loads, 17th Power Systems Computation Conference, (2011).
[20] S. Koch, J.L. Mathieu, D.S. Callaway, Modeling and control of aggregated heterogeneous thermostatically controlled loads for ancillary services, Proceedings of the 17th Power Systems Computation Conference, (2011).
[21] J.L. Mathieu, S. Koch, D.S. Callaway, State estimation and control of electric loads to manage real-time energy imbalance, IEEE Trans. Power Syst. 28 (1) (2013) 430–440.
[22] M.S. Nazir, I.A. Hiskens, Noise and parameter heterogeneity in aggregate models of thermostatically controlled loads, Proceedings of the 20th IFAC World Congress, Toulouse, France, (2017), pp. 8888–8894. Toulouse
[23] J.C. Fuller, K.P. Schneider, D. Chassin, Analysis of residential demand response and double-auction markets, IEEE Power and Energy Society General Meeting, (2011), pp. 1–7.
[24] D.A. Levin, Y. Peres, E.L. Wilmer, Markov Chains and Mixing Times, American Mathematical Society, Providence, RI, 2009.